International Journal of Engineering, Mathematical and Physical Sciences
ISSN: 2517-9934
Vol:9, No:7, 2015

A High-Resolution Refractive Index Sensor Based on a Magnetic Photonic Crystal

Ti-An Tsai, Chun-Chih Wang, Hung-Wen Wang, I-Ling Chang, Lien-Wen Chen

***Abstract*—**In this study, we demonstrate a high-resolution refractive index sensor based on a Magnetic Photonic Crystal (MPC) composed of a triangular lattice array of air holes embedded in Si matrix. A microcavity is created by changing the radius of an air hole in the middle of the photonic crystal. The cavity filled with gyrotropic materials can serve as a refractive index sensor. The shift of the resonant frequency of the sensor is obtained numerically using finite difference time domain method under different ambient conditions having refractive index from n = 1.0 to n = 1.1. The numerical results show that a tiny change in refractive index of Δn = 0.0001 is distinguishable. In addition, the spectral response of the MPC sensor is studied while an external magnetic field is present. The results show that the MPC sensor exhibits a dramatic improvement in resolution.

***Keywords*—**Magnetic photonic crystal, refractive index sensor, sensitivity, high-resolution.

I. Introduction

RECENTLY, the lab-on-a-chip systems based on photonic crystals (PCs) have been developed and fabricated as biological and chemical sensors [1]-[6]. The mechanism for detecting the selective binding between target molecules and capture agents is to measure the change of refractive index (RI). Combing ultra low-loss waveguiding [7] with relatively small footprint microcavities [8], [9] having high quality factor Q, PCs are becoming a popular sensing platform of ultra-compact and large measurement range of RI due to their promising ability to manipulate light by photonic band gap (PBG) [10]. Specifically, the great performance of confining light within a PC microcavity results in high electric field concentration in tiny space, which leads to efficient light interaction with ultra-small area of analyte; therefore, the sensing area effectively shrinks (≤50 μm2) [5], [6]. Besides, the integration of highly-dense optical components in PCs is easily implemented rather than that in bulk optics. For example, Chou et al. [6] have demonstrated an ultracompact PC RI sensor with resolution of $\Delta n = 0.002$ and the sensitivity of less than 200 nm/RIU within the range of $n = 1.0 - 1.5$. However, these proposed sensing schemes of PC microcavities have the disadvantage on their low quality factors because the lightwave could indispensably escape from the planar structures along the out- of- plane direction [11].

Ti-An Tsai, Chun-Chih Wang and Hung-Wen Wang are with the Department of Mechanical Engineering, National Cheng Kung University, Tainan, 70101 Taiwan (e-mail: Kevin77714@me.com, c.c.wang2011@gmail.com, duncanwang9@gmail.com)

I-Ling Chang and Lien-Wen Chen are with the Department of Mechanical Engineering, National Cheng Kung University, Tainan, 70101 Taiwan (e-mail: chenlw@mail.ncku.edu.tw, ilchang@mail.ncku.edu.tw)

Magnetic Photonic Crystal (MPC) is a spatially periodic structure with one of the materials being a magnetic material, such as ferrite. MPCs reveal more properties than the ones made of non-magnetic medium, such as the Faraday effect [12]-[14] and non-reciprocity [15]-[18]. The existence of external magnetic field results in the appearance of the off-diagonal pure imaginary elements in the dielectric tensor, whereas magnitude can be modulated in a way proportional to the external magnetic field intensity [19]-[21]. Jalas et al. [22] have investigated the Faraday effect in ring resonators which leads to the resonance splitting of clockwise and counter-clockwise propagating modes; moreover, the quality factors of both resonant modes increase owing to the splitting phenomena of the degenerate mode in presence of an external magnetic field. H. Kato et al. [12] have demonstrated the localization effect of light in 1D MPC can enhance Faraday rotation more than two orders. The unique property is attributable to the localization effect of light as a result of the multiple interference of light within the magnetic layer.

In this work, we propose a high-resolution RI sensor based on a MPC. The characteristics and sensing properties are investigated numerically by the plane wave expansion (PWE) and finite-difference time-domain (FDTD) methods. Due to the splitting effect of the resonant mode in presence of a external magnetic field, the quality factor Q can be dramatically increased, which can benefit the resolution of the RI sensor. The shift of resonant wavelength can be easily observed in the spectral response under a tiny change in the RI of the surrounding material.

II. Theoretical Background of MPC

To investigate the dispersion relation in periodic structures, we study the propagation of the electromagnetic waves from Maxwell's equations using the PWE method [23]:

$$\nabla \times \left[\varepsilon^{-1}(\vec{r})\nabla \times H(\vec{r})\right] = \frac{\omega^2}{c^2} H(\vec{r}) \tag{1}$$

where $\vec{r}$ is the position vector, $H(\vec{r})$ is the magnetic field, ω is the frequency of light, and c is the light velocity. The dielectric tensor $\varepsilon(\vec{r}) = \varepsilon(\vec{r} + \vec{R})$ is periodic with respect to the real space lattice vector $\vec{R}$. According to Bloch's theorem, the associated parameters in real space can be expressed as a sum of plane waves:

$$\varepsilon^{-1}(\vec{r}) = \sum_{\vec{G}} \eta(\vec{G}) e^{i\vec{G}\cdot\vec{r}} \tag{2}$$

$$H(\vec{r}) = \sum_{\vec{G}} \sum_{\lambda=1,2} h_\lambda(\vec{G}) \hat{e}_\lambda e^{i(\vec{k}+\vec{G})\cdot\vec{r}} \quad (3)$$

where $\vec{G}$ is the reciprocal lattice vector, λ is either 1 or 2, $\vec{k}$ is the Bloch wave vector within the first Brillouin zone, and $\hat{e}_\lambda$ are orthogonal unit vectors perpendicular to $\vec{k}+\vec{G}$. In general, both permittivity tensor ε and permeability tensor μ for magnetic material are anisotropic. At wavelengths in optical regime, the magnetic permeability in most practical cases is reduced to a scalar μ_0, which is the magnetic permeability in vacuum. For example, the permittivity tensors ε for a gyrotropic medium magnetized along x direction can be represented as:

$$\varepsilon = \begin{bmatrix} \varepsilon_{xx} & 0 & 0 \\ 0 & \varepsilon_{yy} & ig \\ 0 & -ig & \varepsilon_{zz} \end{bmatrix} \quad (4)$$

where $\varepsilon_{xx} = \varepsilon_{yy} = \varepsilon_{zz}$ are real, the gyrotropic factor g is responsible for the magneto-optic effect and proportional to the magnetization vector in the first approximation:

$$g = \varepsilon_0 \chi \boldsymbol{B_{ext}} \quad (5)$$

where $\varepsilon_0 = 8.85 \times 10^{-12}$ F/m is the permittivity in vacuum, χ is magneto-optical susceptibility, and $\boldsymbol{B_{ext}}$ is the external magnetic field in unit of Tesla (T). Doing some mathematical manipulations on (1)-(4), we can obtain the following eigenvalue equation in matrix form:

$$\sum_{\vec{G}} H_{\vec{G},\vec{G}'} h_\lambda(\vec{G}') = \frac{\omega^2}{c^2} h_\lambda(\vec{G}) \quad (6)$$

$$H_{\vec{G},\vec{G}'} = \sum_{\vec{G}'} \eta(\vec{G}-\vec{G}') \left|\vec{k}+\vec{G}\right| \left|\vec{k}+\vec{G}'\right| \begin{bmatrix} \hat{e}_2 \cdot \hat{e}'_2 & -\hat{e}_2 \cdot \hat{e}'_1 \\ -\hat{e}_1 \cdot \hat{e}'_2 & \hat{e}_1 \cdot \hat{e}'_1 \end{bmatrix}$$

Once the Fourier coefficients $\eta(\vec{G})$ of the periodic inverse of permittivity tensor $\varepsilon^{-1}(\vec{r})$ has been found, the eigenvalues can be obtained by solving (6).

Fig. 1 depicts the MPC structure under investigation. It is based on a 2D PC composed of infinitely-long air cylindrical holes arranged on a triangular array with lattice constant a = 440 nm, embedded in silicon matrix (n = 3.32). The radius of air holes is r = 0.36 a. If the lightwave travels in the x-z plane perpendicular to the axis of air cylinders in the 2D PC. The (6) can be decoupling into two independent groups for the two respective polarizations of incidence, transverse magnetic (TM) and transverse electric (TE) waves. In the case of TM polarization (the magnetic field is parallel to the axis of air cylinders), (6) can be reduced as:

$$\sum_{\vec{G}'} (\vec{k}+\vec{G}) \cdot (\vec{k}+\vec{G}) \eta(\vec{G}-\vec{G}') h_{\vec{G}'} = \frac{\omega^2}{c^2} h_{\vec{G}} \quad (7)$$

III. Spectral Response of MPC

A microcavity supporting a defect mode is introduced by modifying the radius of an air hole in the middle of the PC. Here, we fill the central air hole with the gyrotropic magnetic material, Bi-YIG ($\varepsilon_{xx} = \varepsilon_{yy} = \varepsilon_{zz} = 4.75$), and the radius of the air hole is set to R_c = 0.55 a as shown in Fig. 1 (a). The PWE method with supercell technique is used to calculate the MPC band structure while the external magnetic field is absent ($g = 0$). According to PWE calculation, the PC structure has a TM gap ranging from normalized frequency 0.241-0.358 in unit of $\omega a/2\pi c$ as shown in Fig. 1 (b).

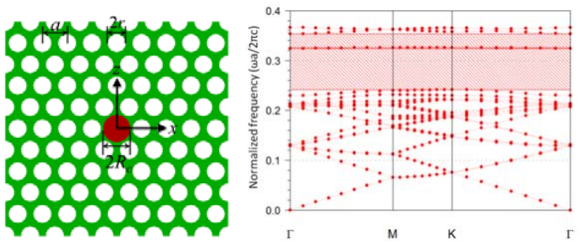

(a) (b)

Fig. 1 (a) The structure of a developed sensor. (b) The band structure of the sensor at the TM wave incidence without applying any external magnetic field. A defect mode appears at f = 0.321 (ωa/2πc) within the bandgap

A defect mode appearing within the PBG corresponds to normalized frequency 0.321 ($\omega a/2\pi c$). In order to retrieve the spectral response of the microcavity, a commercial software, *Rsoft*®, based on FDTD algorithm is employed to simulate the evolves of electromagnetic fields within the MPC structure. In FDTD computations, the structure is a 17 × 17 PC lattice including a defect in the middle of the PC. A Gaussian pulse is used to excited the resonant modes within the cavity and then the evolving fields with time are recorded at several positions of low symmetry. The whole calculating space is surrounded by the perfectly matched layer [24], which absorbs the outgoing waves. Once the temporal data are recorded, the spectral response can be calculated by fast Fourier transform to pick out the resonant peaks of the defect mode. Fig. 2 (a) plots the spectral response of the defect mode of the MPC. One can observe that the resonant frequency of the defect mode, at $f = 0.321$ ($\omega a/2\pi c$) $= 218.86\,\mathrm{THz}$, agrees with the result obtained by PWE method. It is a degenerate mode that has two different modes corresponding to the same frequency. The quality factor $Q = \omega_0/\Delta\omega$ of the microcavity is around 1400, where $\Delta\omega$ is full-width at half-maximum of the resonant peak corresponding to the resonant frequency ω_0. The relative magnetic field distribution at resonance is also plotted in Fig. 2 (b).

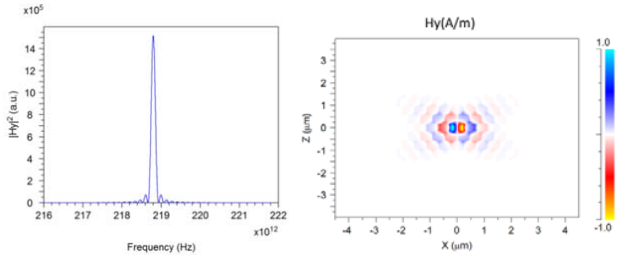

(a) (b)

Fig. 2 (a) The spectral response of the sensor. (b) The spatial distribution of the relative magnetic field normalized to the interval [-1, 1] at resonance (f = 218.86 TH_z) of the microcavity

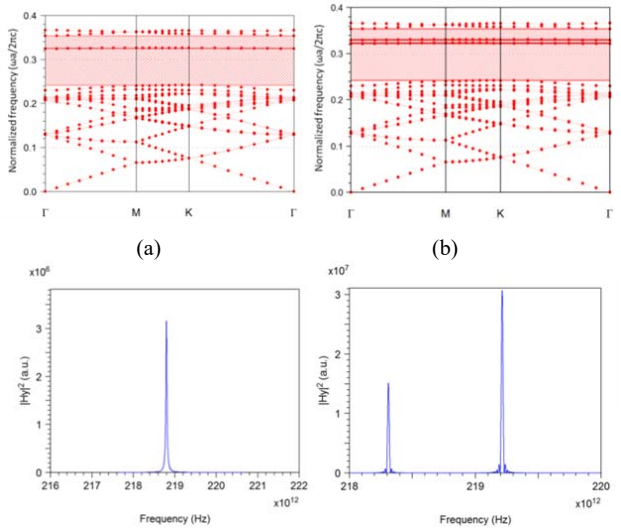

(a) (b)

(c) (d)

Fig. 3 The band structure of the MPC at the TM wave incidence with an external magnetic field (g = 0.1) along: (a) the x-direction; (b) the y-direction. Subplots (c) and (d) are the corresponding spectral responses, respectively

Next, we investigate the impacts of magnetization on band structure and spectral response of the MPC. First, a weak magnetization with gyrotropic factor $g = 0.1$ is considered. Fig. 3 shows band structures under different polarized directions of the external magnetic field. In Fig. 3 (a), it can be seen that a defect mode appears in the PBG when the x-polarized external magnetic field is applied. In this case, the MPC is actually an isotropic PC due to $\varepsilon_{xz} = 0$ and the similar result can be found as shown in Fig. 1 (b). Fig. 3 (b) shows the band structure for the y-polarized magnetic field. In the case of $\varepsilon_{xz} > 0$, the degenerate mode will split into two defect modes, namely, right-hand circular polarization (RCP) and left-hand circular polarization (LCP), whose corresponding normalized frequency are $0.3204(\omega a/2\pi c) = 218.45$ TH_z and $0.3218(\omega a/2\pi c) = 219.41$ TH_z, respectively. For LCP and RCP waves, the corresponding effective RI can be estimated as $n_{\pm} = \sqrt{\varepsilon_{xx} \pm g}$ [25]. The difference in effective RI induces the splitting of the degenerate mode into two circular-polarized modes in the microcavity. The resonant frequency of LCP is higher than that of RCP as a result of the resonant mode of LCP corresponding to the lower effective RI [11]. In addition, it can be seen that the RI n_+ for RCP wave increases and RI n_- for LCP wave decrease with the increasing in magnitude of magnetization, which means that the resonant frequencies for RCP and LCP wave move in opposite direction accordingly. It is worth noting that the resonant peaks will emerge into photonic pass bands when the gyrotropic factor g is too large (which is not shown here). From the spectral response as shown in Fig. 3 (c), there is only a resonant peak at frequency of 218.86 TH_z. In Fig. 3 (d), two resonant peaks can be observed with frequencies at 218.45 TH_z and 219.41 TH_z for RCP and LCP wave, respectively.

IV. Utilization of MPC Sensors and Their Performance

We infiltrate the air holes of MPC with several different analyte materials with refractive index ranging from $n = 1.0$ to $n = 1.1$ in 0.01 interval. The spectral response are calculated as shown in Fig. 4 When the air holes of the MPC are filled with the analyte material, the refractive index distribution of the MPC is changed, which causes the shift of the resonant frequency. Fig. 4 (a) shows the spectral response as the external magnetic field is applied to x-direction at gyrotropic factor $g = 0.6$. The resonant frequencies are red-shiftted as the increasing of analyze RI. Fig. 4 (b) shows the RCP (B-region) and LCP (A-region) modes for y-polarized external magnetic field, respectively. We can observe that they have similar trends with Fig. 4 (a). Because the increasing in RI of analyte reduces the RI contrast between the Si background and analyte material, the frequency of the resonant mode move towards the lower bandgap. In addition, the reduction in the RI contrast will deteriorate the confinement ability of the electromagnetic field, which results in small leaky energy from the microcavity and then slightly suppress the Q factor as shown in Fig. 5 (a).

The sensitivity S of the MPC sensor is defined as the ratio of the resonant shift in wavelength to RI variations of the analyte ($S \equiv \Delta\lambda/\Delta n$). Fig. 5 (b) depicts the relationship between resonant shift $\Delta\lambda$ and RI of analyte under magnetization with different polarizations. It can be seen that the data are fit using linear function and the slope of each line actually represents the sensitivity of the MPC sensor in the corresponding polarization of external magnetic field.

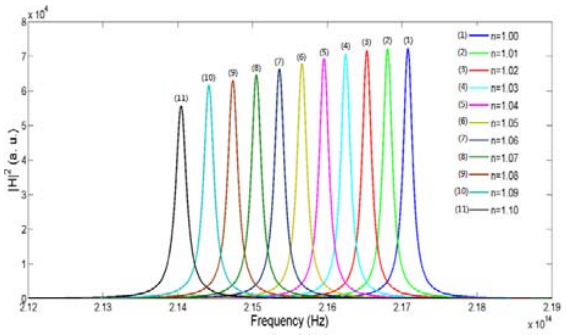

(a)

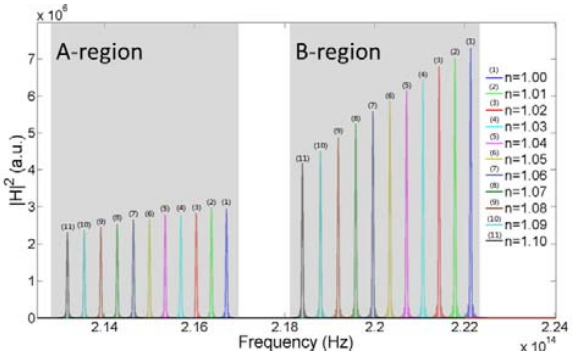

(b)

Fig. 4 The frequency shift of the defect mode for the sensor with g = 0.6 when the RI of ambience increases from n = 1.0 to n = 1.1 in steps of 0.01. (a) The degenerate mode when the external magnetic field is applied to the x-direction. (b) The RCP (B-region) and LCP (A-region) mode when the external magnetic field is applied to the y-direction

Numerical results show that S is 194.08 (230.98) in unit of nm/RIU when the external magnetic field is applied in x-direction (y-direction). Though, the external magnetic field is beneficial to enhance sensitivity, the splitting resonant modes can lead some difficulties in identifications. For example, Fig. 6 (a) shows the frequency response when the external magnetic field is applied in y-direction and the gyrotropic factor is set to $g = 0.2$. Several analyte with RI from 1.0 to 1.10 in increments of 0.02 are investigated. Each of them exhibits two resonant peaks in frequency response as shown in Fig. 6 (a). Denote the resonant frequency of the LCP (RCP) mode as f_L (f_R), and the difference between the two resonant frequencies as $\Delta f = f_L - f_R$. It is worth mentioning that the separation in frequency between the LCP and RCP mode enlarges linearly with the gyrotropic factor g. That is, the stronger the external magnetic field is, the larger Δf can be obtained owing to the proportional relationship between the magnetic field and gyrotropic factor g as indicated in (5). The gray area in Fig. 6 (a) shows that if RI of analyte is gradually increasing over than 1.04, The LCP modes overlaps with RCP ones if g is too small as shown in the grey area. This will cause ambiguity in identifying the RI of analyte and limit the range of measurement. To facilitate the difficulty, one convenient way is to tune the gyrotropic factor up to $g = 0.6$ by increasing the magnitude of external magnetic field as shown in Fig. 6 (b). Therefore, the free spectral range between LCP and RCP modes now is separated sufficiently to avoid the ambiguity and the range of measurement can be enlarged.

In order to demonstrate the high resolution of the RI sensor is feasible, several common gases with respect to industrial safety are analyzed. In general, the RI of the gas is usually lower than the liquid and solid, and the differences of RI between gases are also quite small, which brings difficulties in identification. For example, the RI of helium is 1.000036, hydrogen is 1.00014, ammonia is 1.000377 and so on. Fig. 7 shows the result of measurement for six different gases. It can be found that the high resolution characteristics of the sensor can distinguish the above-mentioned gases, which means that the sensor resolution can reach to $\Delta n = 0.0001$. This is a great benefit to chemical gas sensing. The enhancement in sensitivity by magneto-optic effect makes our device a promising candidate for highly sensitive, densely integrated, and label-free optical detection system.

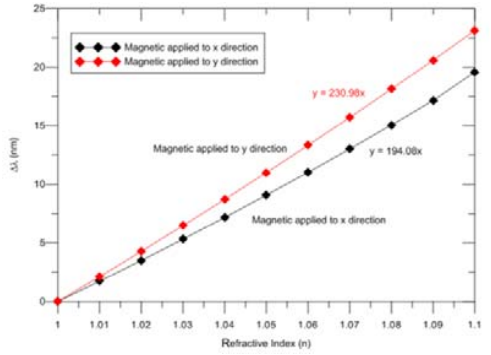

(a)

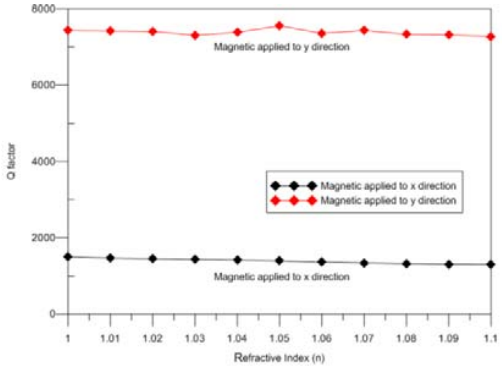

(b)

Fig. 5 (a) The quality factor of a developed sensor. (b) The deviation in resonant wavelength ($\Delta\lambda = \lambda - \lambda_0$, where λ_0 is the resonant wavelength at n = 1.0) when the RI of ambience increases from n = 1.0 to n = 1.1 in steps of 0.01

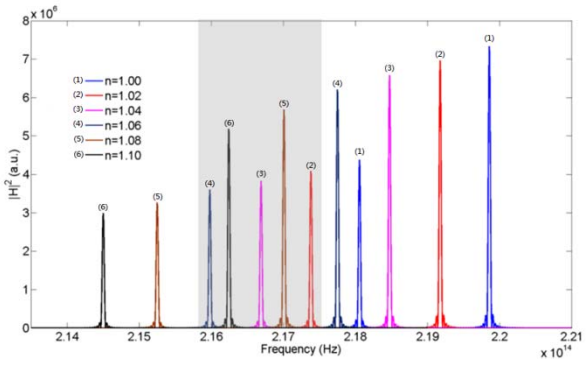

(a)

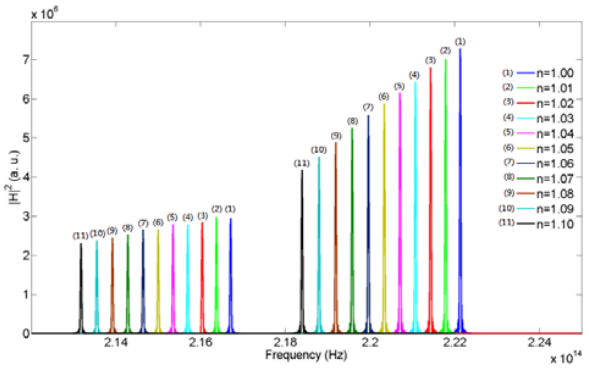

(b)

Fig. 6 Impacts of the gyrotropic parameter g on the defect modes. (a) Resonant frequencies of defect modes versus the RI of ambience with g = 0.2. The LCP modes overlaps with RCP ones if g is too small as shown in the grey area. (b) Resonant frequencies of defect modes versus the RI of ambience with g = 0.6

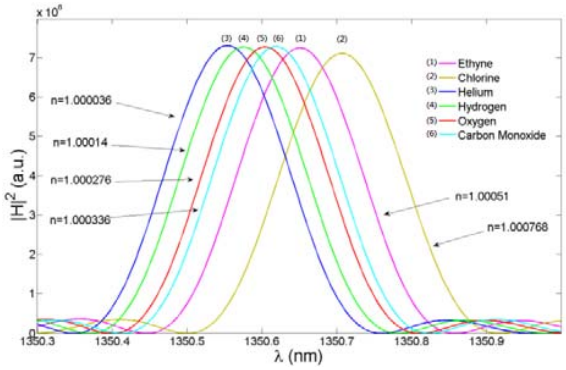

Fig. 7 The capability demonstration of a developed sensor for real gases sensing

V. Conclusion

In this paper, we in detail calculated and analyzed the effects of the polarizations of external magnetic field and gyrotropic factor on sensitivity and resolution of the MPC sensor using FDTD method. It was found that one can increase or decrease free spectral range Δf by tuning the magnitude of external magnetic field. Numerical results showed that the MPC sensor exhibits sensing sensitivity of $\Delta\lambda/\Delta n$ = 230 nm/RIU, high factor of Q = 7300 in average, and resolution of Δn = 0.0001 in RI measurement. The sensor can be used to measure gas, fluids, or chemicals due to the high resolution characteristic.

Acknowledgment

The partial support by the National Science Council of Taiwan under Grant NSC 101-2221-E-006-104-MY3 is gratefully acknowledged.

References

[1] J. O. Grepstad, P. Kaspar, O. Solgaard, I. R. Johansen, A. S. Sudbø, "Photonic-crystal membranes for optical detection of single nano-particles, designed for biosensor application", *Opt. Exp.* 2012, 20, 7954-7965.
[2] C. Kang, C. T. Phare, Y. A. Vlasov, S. Assefa, S. M. Weiss, "Photonic crystal slab sensor with enhanced surface area", *Opt. Exp.* 2010, 18, 27931-27937.
[3] S. Kita, K. Nozaki, T. Baba, "Refractive index sensing utilizing a cw photonic crystal nanolaser and its array configuration", *Opt. Exp.* 2008, 16, 8175-8180.
[4] U. Bog, C. L. C. Smith, M. W. Lee, S. Tomljenovic-Hanic, C. Grillet, C. Monat, L. O'Faolain, C. Karnutsch, T. F. Krauss, R. C. McPhedran, B. J. Eggleton, "High-Q microfluidic cavities in silicon-based two-dimensional photonic crystal structures", *Opt. Lett.* 2008, 33, 2206-2208.
[5] M. R. Lee, P. M. Fauchet, "Two-dimensional silicon photonic crystal based biosensing platform for protein detection", *Opt. Exp.* 2007, 15, 4530-4535.
[6] E. Chow, A. Grot, L. W. Mirkarimi, M. Sigalas, G. Girolami, "Ultracompact biochemical sensor built with two-dimensional photonic crystal microcavity", *Opt. Lett.* 2004, 29, 1093-1095.
[7] A. Mekis, J. C. Chen, I. Kurland, S. Fan, P. R. Villeneuve, J. D. Joannopoulous, "High transmission through sharp bends in photonic crystal waveguides", *Phys. Rev. Lett.* 1996, 77, 3787-3790.
[8] P. R. Villeneuve, S. Fan, J. D. Joannopoulos, "Microcavities in photonic crystals: Mode symmetry, tunability, and coupling efficiency", *Phys. Rev. B* 1996, 54, 7837-7842.
[9] Y. Akanhane, T. Asano, B. S. Song, S. Noda, "High-Q photonic nanocavity in a two-dimensional photonic crystal", *Nature* 2003, 425, 944-947.
[10] J. D. Joannopoulos, R. D. Meade, J. N. Winn, *Photonic Crystals: Molding the Flow of Light*, Princeton University Press, 1995.
[11] O. Painter, J. Vučkovič, A. Scherer, "Defect modes of a two-dimensional photonic crystal in an optically thin dielectric slab", *J. Opt. Soc. Am. B* 1999, 16, 275-285.
[12] H. Kato, T. Matsushita, A. Takayama, M. Egawa, "Theoretical analysis of optical and magneto-optical properties of one-dimensional magnetophotonic crystals", *J. Appl. Phys.* 2003, 93, 3906-3911.
[13] S. N. Kurilkina, M. V. Shuba, "Propagation and transformation of the light waves in magnetoactive periodic structures", *Opt. Spectrosc.* 2002, 93, 918-923.
[14] A. G. Zhdanov, A. A. Fedyanin, O. A. Aktsipetrov, D. Kobayashi, H. Uchida, M. Inoue, "Enhancement of Faraday rotation at photonic-band-gap edge in garnet-based magnetophotonic crystals", *J. Magn. Magn. Mater.* 2006, 300, e253-e256.
[15] P. A. Belov, S. A. Tretyakov, A. J. Viitanen, "Nonreciprocal microwave band-gap structures", *Phys. Rev. E* 2002, 66, 016608.
[16] A. Figotin, I. Vitebskiy, "Electromagnetic unidirectionality in magnetic photonic crystals", *Phys. Rev. B* 2003, 67, 165210.
[17] W. Śmigaj, J. Romero-Vivas, B. Gralak, L. Magdenko, B. Dagens, M. Vanwolleghem, "Magneto-optical circulator designed for operation in a uniform external magnetic field", *Opt. Lett.* 2010, 35, 568-570.
[18] Z. Wang, L. Shen, Z. Yu, X. Zhang, X. Zheng, "Highly efficient photonic-crystal splitters based on one-way waveguiding", *J. Opt. Soc. Am. B* 2013, 30, 173-176.
[19] I. H. H. Zabel, D. Stroud, "Photonic band structures of optically anisotropic periodic arrays", *Phys. Rev. B* 1993, 48, 5004-5012.
[20] A. Soltani Vala, B. Rezaei, M. Kalafi, "Tunable defect modes in 2D photonic crystals by means of external magnetic fields", *Physica B* 2010, 405, 2996-2998.
[21] H. Wang, Y. Luo, Y. T. Wang, H. B. Zhang, Y. T. Fang, "Splitting of defect-mode in one-dimensional magnetic photonic crystal", *Physica B* 2011, 406, 2977-2981.
[22] D. Jalas, A. Petrov, M. Krause, J. Hampe, M. Eich, "Resonance splitting in gyrotropic ring resonators", *Opt. Lett.* 2010, 35, 3438-3440.
[23] K. Sakoda, *Optical Properties of Photonic Crystals*, Springer, 2001.
[24] S. D. Gedney, "An anisotropic perfectly matched layer-absorbing medium for the truncation of FDTD lattices", *IEEE Trans. Antennas Propagat.* 1996, 44, 1630-1639.
[25] B. E. A. Saleh, M. C. Teich, *Fundamentals of Photonics*, Wiley-Interscience, 2007.